Asteroseismology of KIC 8263801:Is it a member of NGC 6866 and a red clump star?

Tang, Yanke; Basu, Sarbani; Davies, Guy R.; Bellinger, Earl P.; Gai, Ning

DOI:
10.3847/1538-4357/aadcf2

The Astrophysical Journal, 866:59 (9pp), 2018 October 10 https://doi.org/10.3847/1538-4357/aadcf2

Asteroseismology of KIC 8263801: Is It a Member of NGC 6866 and a Red Clump Star?

Yanke Tang[1,2,3], Sarbani Basu[2], Guy R. Davies[4], Earl P. Bellinger[2,5,6,7], and Ning Gai[1,2,3]
[1] College of Physics and Electronic information, Dezhou University, Dezhou 253023, People's Republic of China
tyk@dzu.edu.cn, sarbani.basu@yale.edu, ning.gai@hotmail.com
[2] Department of Astronomy, Yale University, P.O. Box 208101, New Haven, CT 06520-8101, USA
[3] Shandong Provincial Key Laboratory of Biophysics, Dezhou University, Dezhou 253023, People's Republic of China
[4] School of Physics and Astronomy, University of Birmingham, Birmingham, B15 2TT, UK
[5] Max-Planck-Institut für Sonnensystemforschung, Justus-von-Liebig-Weg 3, D-37077 Göttingen, Germany
[6] Stellar Astrophysics Centre, Department of Physics and Astronomy, Aarhus University, Ny Munkegade 120, DK-8000 Aarhus C, Denmark
[7] Institut für Informatik, Georg-August-Universität Göttingen, Goldschmidtstrasse 7, D-37077 Göttingen, Germany
Received 2018 July 4; revised 2018 August 21; accepted 2018 August 22; published 2018 October 11

Abstract

We present an asteroseismic analysis of the *Kepler* light curve of KIC 8263801, a red-giant star in the open cluster NGC 6866 that has previously been reported to be a helium-burning red-clump (RC) star. We extracted the frequencies of the radial and quadrupole modes from its frequency power spectrum and determined its properties using a grid of evolutionary models constructed with MESA. The oscillation frequencies were calculated using the GYRE code and the surface term was corrected using the Ball & Gizon prescription. We find that the star has a mass of $M/M_{\odot} = 1.793 \pm 0.072$, age $t = 1.48 \pm 0.21$ Gyr, and radius $R/R_{\odot} = 10.53 \pm 0.28$. By analyzing the internal structure of the best-fitting model, we infer the evolutionary status of the star KIC 8263801 as being on the ascending part of the red-giant branch, and not on the RC. This result is verified using a purely asteroseismic diagnostic, the $\epsilon_c - \Delta\nu_c$ diagram which can distinguish red-giant branch stars from red-clump stars. Finally, by comparing its age with NGC 6866 ($t = 0.65 \pm 0.1$ Gyr), we conclude that KIC 8263801 is not a member of this open cluster.

Key words: stars: evolution – stars: oscillations – stars: solar-type

1. Introduction

Since the NASA *Kepler* spacecraft was successfully launched in 2009 March, stellar pulsations of over 10,000 red giants have been observed (Borucki et al. 2009, 2010; De Ridder et al. 2009; Bedding et al. 2010; Gilliland et al. 2010; Koch et al. 2010; Balona et al. 2013a, 2013b; Abedigamba 2016). The red-giant (RG) star KIC 8263801 is one of these. Located in the field of NGC 6866—the youngest of the four clusters observed by *Kepler*—the pulsations of KIC 8263801 have been observed with a signal-to-noise ratio that is good enough to constrain its fundamental parameters. Balona et al. (2013a) identified 704 stars in this cluster, of which 23 are RG stars showing solar-like oscillations. Abedigamba (2016) used median gravity-mode period spacings (ΔP) to search for red-clump (RC) stars among the RG stars showing solar-like oscillations. Based on its $\Delta P = 173.7 \pm 6.4$ s, Abedigamba (2016) determined that KIC 8263801 is a secondary red-clump (SRC) star, which is massive enough to have ignited helium burning in a nondegenerate core. However, the signal-to-noise of KIC 8263801 is not enough to derive an accurate ΔP. In this paper, we perform an asteroseismic analysis of the mode frequencies in order to determine the evolutionary state of KIC 8263801.

One of the major problems in the study of open clusters is to determine which stars are members of the clusters and which stars are not. Although, KIC 8263801 has been classified as a nonmember of NGC 6866 based on photometric distance membership determination and proper motions (Balona et al. 2013a), Balona et al. (2013a) and Abedigamba (2016) pointed out that they cannot be quite sure of the membership with only a single method. Abedigamba (2016) stated that NGC 6866 is roughly located in the direction of solar apex, which means that all stars (members and nonmembers) have similar proper motions. One cannot use proper motion to discriminate between members and nonmembers. No radial velocity measurements for stars located in the field of NGC 6866 are available to help in discriminating between members and nonmembers. The only method left in discriminating between members and nonmembers in the field of NGC 6866 is the photometric distance method. However, with only a single method, one cannot be quite sure of the membership. Balona et al. (2013a) also attempted to identify cluster members using their proper motions but found very poor discrimination between members and nonmembers. Hence, another focus of this paper is to revisit the issue of the cluster nonmembership of KIC 8263801 by means of comparing the age of the star determined through asteroseismic modeling and the age of the cluster.

Asteroseismology is an efficient tool for studying the internal structures of stars through their global oscillations (Tang et al. 2008a, 2008b; Chaplin et al. 2011, 2014a, 2014b; Tang & Gai 2011; Pinsonneault et al. 2014; Silva Aguirre et al. 2015, 2017; Bellinger et al. 2016, 2017). Basic stellar properties such as mass and age can be derived this way (e.g., Basu et al. 2010a, 2010b; Yildiz et al. 2017). For the stars with solar-like oscillations, when the signal-to-noise ratios in the seismic data are insufficient to allow robust extraction of individual oscillation frequencies, it is still possible to extract estimates of the large frequency separation ($\Delta\nu$) and the frequency of maximum oscillation power ($\nu_{\rm max}$). The large separation $\Delta\nu$ is the separation between oscillation modes with the same angular

degree and consecutive radial orders (Tassoul 1980):

$$\Delta\nu_l(n) = \nu_{n,l} - \nu_{n-1,l}, \quad (1)$$

which scales to a very good approximation with the square root of the stellar mean density (Kjeldsen & Bedding 1995; Stello et al. 2011):

$$\frac{\Delta\nu}{\Delta\nu_\odot} \simeq \sqrt{\frac{M/M_\odot}{(R/R_\odot)^3}}. \quad (2)$$

The other, $\nu_{\rm max}$, is related with the cutoff frequency for acoustic waves in an isothermal atmosphere, which scales with surface gravity g and effective temperature $T_{\rm eff}$ (Brown et al. 1991; Kjeldsen & Bedding 1995) as

$$\frac{\nu_{\rm max}}{\nu_{\rm max\,\odot}} \simeq \left(\frac{g}{g_\odot}\right)\left(\frac{T_{\rm eff}}{T_{\rm eff,\odot}}\right)^{-1/2} \quad (3)$$

with the solar values $\Delta\nu_\odot = 135\ \mu$Hz and $\nu_{\rm max\odot} = 3090\ \mu$Hz (Huber et al. 2009, 2011; Chaplin et al. 2014a) providing the absolute calibration in this study. These scaling relations have been applied with success to main-sequence and subgiant stars as well as to stars on the red-giant branch (RGB) and helium burning (HeB) stars. According to the above scaling relations, asteroseismology can help constrain the global parameters of a star with reasonable precision. For more evolved stars, the scaling relation has reduced accuracy (Gualme et al. 2016; Guggenberger et al. 2016, 2016).

The classical Hertzsprung–Russell diagram (HRD) shows that red-giant branch stars (burning hydrogen in a shell around an inert helium core) and red-clump stars (with helium-core and hydrogen-shell burning) occupy overlapping parameter spaces (e.g., Elsworth et al. 2017). Although these stars have different internal conditions, which we can observe indirectly, they have similar surface characteristics—such as effective temperature, surface gravity, and total luminosity, which can be observed directly. Hence, from classical observations such as these, it is often not possible to distinguish between RGB stars of about 10–12 $R_\odot$ and HeB stars of a similar radius. The distinction is easier in clusters, but even in clusters there is room for ambiguity. This is where asteroseismology is useful. Space missions such as *Kepler* have made red-giant asteroseismology possible, with *Kepler* providing long time series data that allow the frequency resolution needed to determine frequencies of individual oscillation modes of red giants (Bedding et al. 2011; Beck et al. 2011; Kallinger et al. 2012; Handberg & Lund 2017). Nonradial modes in red giants exhibit mixed character; they behave like gravity modes (g modes) in the interior but like acoustic modes (p modes) in the outer layers. The asteroseismic properties of RGB and HeB stars are quite different (Bedding et al. 2011; Kallinger et al. 2012; Elsworth et al. 2017) and hence are useful in determining the evolutionary state of red giants. This is what we do in this paper. We extract the mode frequencies of the radial and quadrupole modes KIC 8263801, construct models that match the frequencies, and use those to identify the evolutionary state of the star to determine whether or not it is a member of NGC 6866. Additionally, we also use a purely asteroseismic diagnostic to confirm its evolutionary state. We do not use the dipole modes since the frequencies and frequency spacings of the most g-type modes are determined by the details of the profile of the buoyancy frequency, which depends on uncertain model parameters such as the exact treatment of overshoot etc. Radial ($l = 0$) and quadrupole ($l = 2$) mode frequency are more robust in this respect.

In this paper, we extract the mode frequencies of the radial and quadrupole modes by "peak bagging" the frequency power spectrum observed by *Kepler* in Section 2. We use these individual mode frequencies to constrain models of KIC 8263801, identify the evolutionary state of the star, and confirm that it is not a member of the open cluster NGC 6866 in Sections 3 and 4. Conclusions are presented in Section 5.

2. Observational Data

2.1. Asteroseismic Fitting

We extract the mode frequencies of the radial and quadrupole modes using the KASOC unweighted power spectrum (Handberg & Lund 2014) containing the *Kepler* data spanning Quarters 1–3, 6–11, and 14 shown in Figure 1 and Figure 2. The data result in a frequency resolution of ≈9 nHz. First guesses to the frequencies of the radial and quadrupole modes were obtained using a fit of the asymptotic expression for radial modes to the power spectrum (Davies & Miglio 2016). Peak bagging for these modes was done using the procedure, and the code, of Davies et al. (2016). As is described in Davies et al. (2016), an unsupervised machine-learning Bayesian scheme is used to obtain a set of probabilities to assess whether or not a mode had been detected in the data. We use the ratio of the probability of a detection over the probability of no detection (the Bayes factor). If the natural log of the Bayes factor is high, we accept the mode. Only five radial orders passed the quality test shown in Figure 2. The fitted frequencies are given in Table 1. We derive the values of large separation $\Delta\nu = 5.35 \pm 0.01\ \mu$Hz and $\nu_{\rm max} = 56.2 \pm 0.4\ \mu$Hz shown in Table 2, which are consistent with the results obtained by Abedigamba (2016).

2.2. Classical Observations

The effective temperature $T_{\rm eff} = 4766$ K, metallicity $[{\rm Fe/H}] = 0.016$ dex, and surface gravity $\log g = 2.487$ (dex) of KIC 8263801 were obtained from Brown et al. (2011). The stated uncertainties of these quantities were 200 K in $T_{\rm eff}$ and 0.4 dex in $\log g$. Although an uncertainty for the metallicity was not reported, the uncertainties were expected to be high. Huber et al. (2014) subsequently presented revised stellar properties for 196 468 *Kepler* targets, including this one. They give $T_{\rm eff} = 4974 \pm 161$ K, metallicity $[{\rm Fe/H}] = 0.016 \pm 0.30$ (dex), and $\log g = 2.662 \pm 0.03$ for this star. We use these observational constraints as the error boxes, as shown in Figure 3, where maximum (black) uncertainty corresponds to the observational value from the *Kepler* website and minimum (green) uncertainty corresponds to the observational value given by Huber et al. (2014). Due to the location of KIC 8263801 in the field of NGC 6866, we also consider that it may have a similar metallicity to this cluster. Bostanci et al. (2015) and Balona et al. (2013a) give the metallicity of the cluster as being about the solar value, whereas Loktin et al. (1994) derived $[{\rm Fe/H}] = 0.10$ (dex) via photometry from Hoag et al. (1961). All nonasteroseismic observational constraints are listed in Table 3.

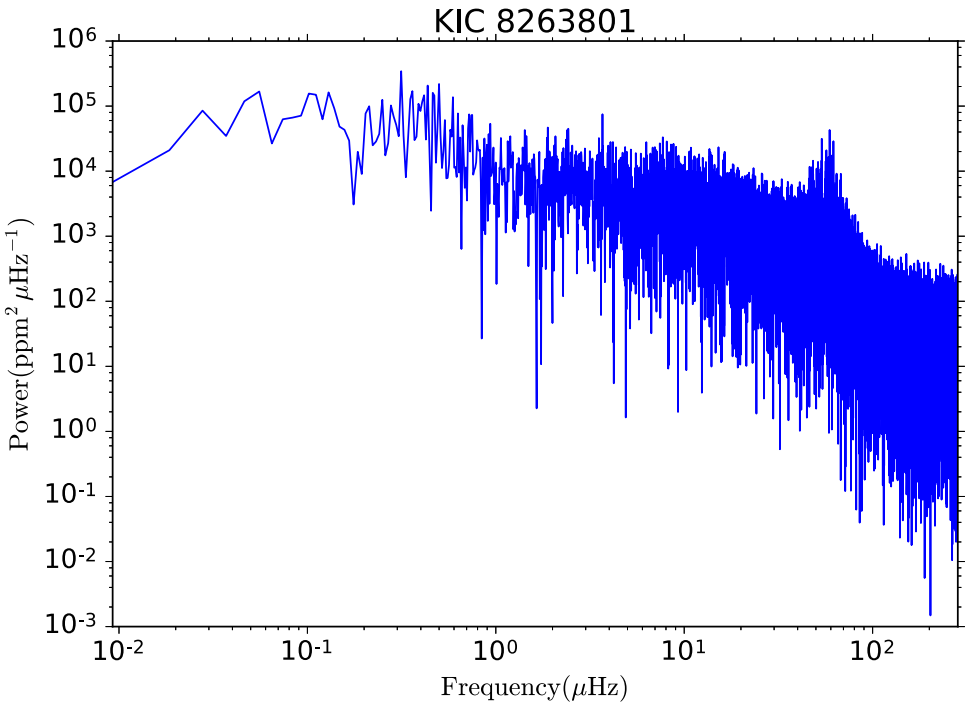

Figure 1. Power spectrum for KIC 8263801 from *KEPLER* photometry.

Table 1
Asteroseismic Observational Frequencies of KIC 8263801

n	l	Value	Error
8	0	43.242	0.068
9	0	48.294	0.020
10	0	53.705	0.017
11	0	59.126	0.012
12	0	64.502	0.063
8	2	41.64	0.86
9	2	47.573	0.032
10	2	52.810	0.069
11	2	58.352	0.020
12	2	63.75	0.12

Table 2
Asteroseismic Global Parameters of KIC 8263801

Observable Variable	Value	Source
Large separation $\Delta\nu$	5.35 ± 0.01	(1)
	5.3541	(2)
$\nu_{\rm max}$	56.2 ± 0.4	(1)
	56.422	(2)

References. (1) This paper; (2) Abedigamba (2016).

3. Modeling KIC 8263801

3.1. Constructing Models

Having values of $\nu_{\rm max}$, $\Delta\nu$, and $T_{\rm eff}$, the scaling relations (Equations (2) and (3)) can be used to calculate the mass, luminosity, and radius of the star. Using these scaling relations, Abedigamba (2016) determined that KIC 8263801 has a mass of $M/M_\odot = 1.86$ and luminosity of $\log(L/L_\odot) = 1.7555$. However, more robust estimates of these quantities can be obtained by means of a grid-based analysis, which constrains stellar parameters by searching among a grid of evolutionary models to get a best fit for observed values of $\nu_{\rm max}$, $\Delta\nu$, $T_{\rm eff}$, and metallicity (e.g., Basu et al. 2010a, 2011; Gai et al. 2011; Chaplin et al. 2014a, 2014b). Since we have extracted the individual frequencies of the star in addition to the global asteroseismic parameters, we can use grid-based modeling to obtain better results by selecting models that fit the observed frequencies and not just the global asteroseismic parameters $\nu_{\rm max}$ and $\Delta\nu$.

We use the MESA stellar evolution code (Modules for Experiments in Stellar Astrophysics, Paxton et al. 2011, 2013, version 8845) to construct models. We employ the default MESA input options unless otherwise stated. We evolve each pre-main-sequence model until its nuclear luminosity first reaches 99.9% of the total luminosity, which we define as being zero-age main sequence (ZAMS). We use the Eddington T-τ atmosphere from ZAMS onward. Each track is then evolved from ZAMS to asymptotic giant branch as shown in Figure 3. We treat the convection zone by the standard mixing-length theory of Cox & Giuli (1968) with the mixing-length parameter $\alpha_{\rm MLT} = 2.0$ (Wu & Li 2016).

Referring to the mass value derived by Abedigamba (2016), we make models in a range of initial masses from $1.7\,M_\odot$ to $2.0\,M_\odot$ with a step of $0.02\,M_\odot$. According to the discussion of metallicity presented in Section 2.2, we allow the initial heavy element abundances Z_i to range from 0.01 to 0.025 with a step of 0.005 as shown in Table 4 via

$$\log[{\rm Z/X}] \simeq [{\rm Fe/H}] + \log[{\rm Z/X}]_\odot, \quad (4)$$

where $[{\rm Z/X}]_\odot = 0.023$ (Grevesse & Sauval 1998). All input parameters are shown in Table 4. Once the initial heavy element abundance Z_i is determined, the dependence of initial helium mass fraction Y_i on Z_i can be set using a linear helium enrichment expression with the primordial helium abundance

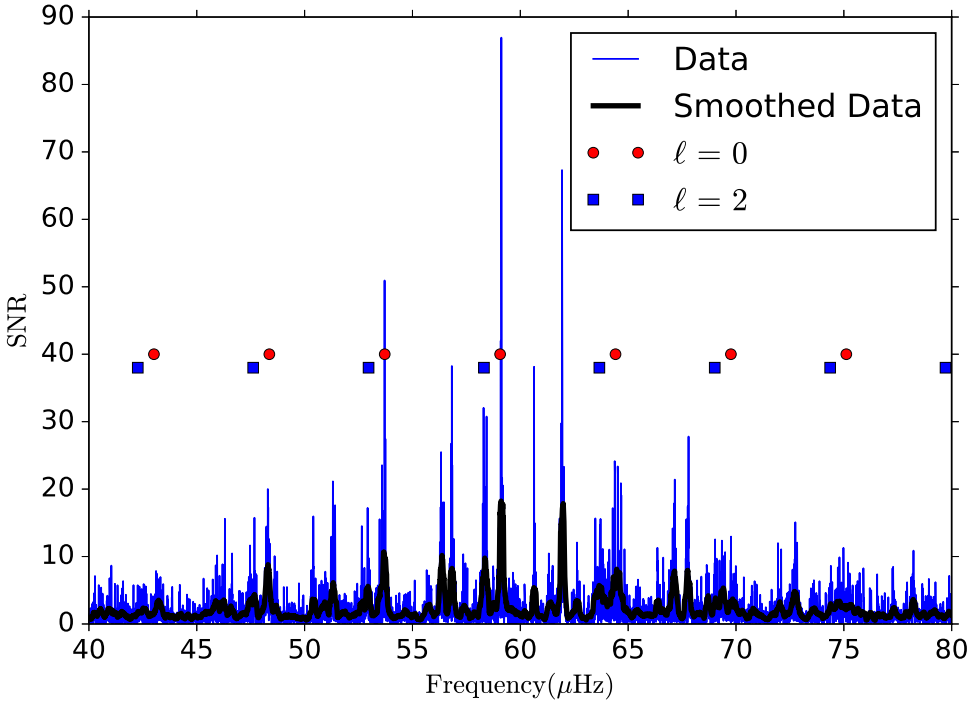

Figure 2. Identified p-mode oscillation spectrum of the red giant KIC 8263801 in function of frequency. The (blue) thin and (black) thick lines denote the power spectrum before and after smoothing.

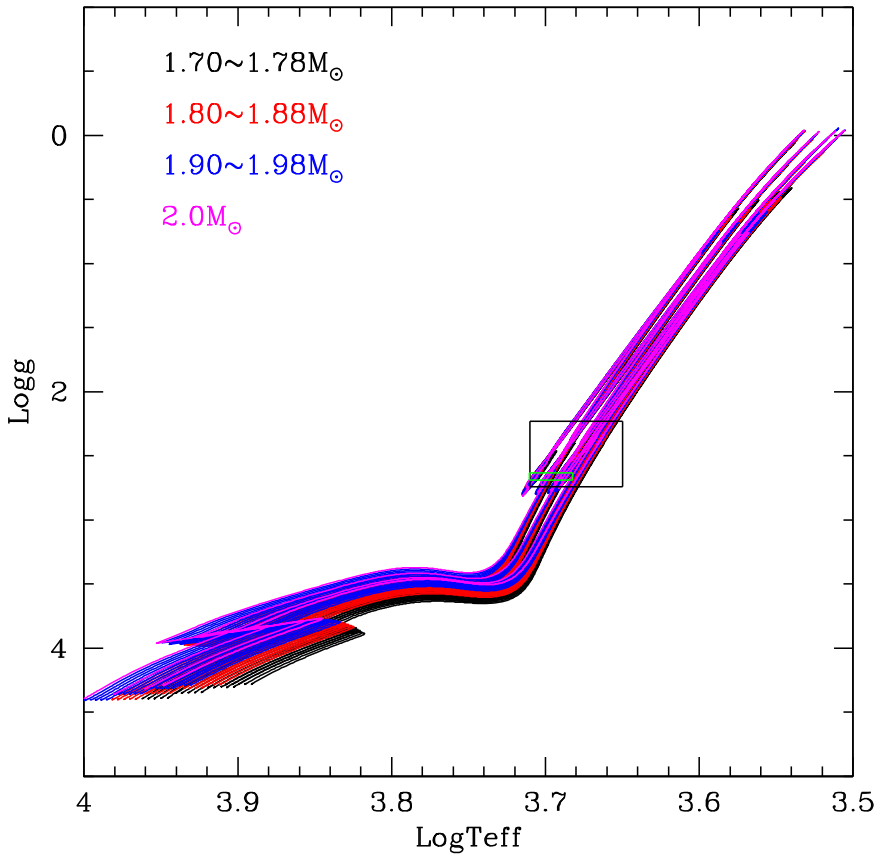

Figure 3. Evolutionary tracks of models constructed for this work. The large (black) error box corresponds to observational values from the *Kepler* website, while the small (green) error box corresponds to the revised observational value given by Huber et al. (2014).

Table 3
Nonasteroseismic Data of KIC 8263801

Observed Variable	Value	Source
Effective temperature $T_{\rm eff}$ (K)	4766	(1)
	4974 ± 161	(2)
Metallicity [Fe/H]	0.016	(1)
	0.016 ± 0.30	(2)
Log g (dex)	2.487	(1)
	2.662 ± 0.03	(2)

References. (1) Brown et al. (2011); (2) Huber et al. (2014).

Table 4
Input Parameters for Models

Variable	Minimum Value	Maximum Value	Step Size
Initial Mass ($M_{\odot}$)	1.70	2.00	0.02
Initial Heavy Element Abundance Z_i	0.01	0.025	0.005

$Y_p = 0.24$ and the slope $\Delta Y/\Delta Z = 2$ (Demarque et al. 2004; Basu et al. 2010a) by the following:

$$Y_i = Y_p + \frac{\Delta Y}{\Delta Z} Z_i. \tag{5}$$

Finally, the initial hydrogen element abundance X_i is obtained via

$$X_i = 1 - Y_i - Z_i. \tag{6}$$

3.2. Calculating Mode Frequencies

We use the GYRE oscillation code (Townsend & Teitler 2013) to calculate the mode frequencies of the models. Due to surface effects, there is a systematic offset between the observed and model frequencies (e.g., Christensen-Dalsgaard 1984). In order to obtain the accurate modeling of solar-like oscillations, we should use a systematic shift to correct the model frequencies. A number of ways have been proposed to correct the frequencies for the surface issues (usually called the "surface-term" correction). The most common way to correct for the surface term for stellar models is the method proposed by Kjeldsen et al. (2008). They note that the offset between observed and best model frequencies turns out to be closely fitted by a power law. However, there are issues with many of the surface-term corrections, even for main-sequence stars; and most models perform very badly in the subgiant and red-giant region. Schmitt & Basu (2015) found that the two-term model proposed by Ball & Gizon (2014) works better than other models across a large portion of the HR diagram, and consequently we adopt that for this work.

4. Results and Discussions

We show the evolutionary track of our models in Figure 3. The figure also shows the two error boxes. $T_{\rm eff} = 4766 \pm 200$ K and $\log g = 2.487 \pm 0.4$ have been used for the large error box while $T_{\rm eff} = 4974 \pm 161$ K and $\log g = 2.662 \pm 0.03$ for the smaller error box. We find that many models fall into the two error boxes. In order to obtain the best-fit model for KIC 8263801 from among these models, we calculated the likelihood for each model and determined the model with the highest likelihood. The likelihood function is defined as

$$\mathcal{L} = \left(\prod_{i=1}^{n} \frac{1}{\sqrt{2\pi}\,\sigma_i}\right) \cdot \exp\left\{-\frac{\chi^2}{2}\right\} \tag{7}$$

where

$$\chi^2 = \sum_{i=1}^{n} \left(\frac{q_i^{\rm obs} - q_i^{\rm model}}{\sigma_i}\right)^2. \tag{8}$$

with the quantity $q_i^{\rm obs}$ indicating the observed $T_{\rm eff}$, [Fe/H], and frequency $\nu_{n,\,l}$; while the $q_i^{\rm model}$ corresponds to these values of the model. The quantity σ_i represents the observational error of $q_i^{\rm obs}$. In the study, we use the function as follows:

$$\mathcal{L}(T_{\rm eff},\,[{\rm Fe/H}],\,\nu) = \mathcal{L}_{T_{\rm eff}} \cdot \mathcal{L}_{[{\rm Fe/H}]} \cdot \mathcal{L}_{\nu} \tag{9}$$

where

$$\mathcal{L}_{T_{\rm eff}} = \frac{1}{\sqrt{2\pi}\,\sigma_{T_{\rm eff}}} \cdot \exp\left\{-\frac{(T_{\rm eff,obs} - T_{\rm eff,model})^2}{2\sigma_{T_{\rm eff}}^2}\right\} \tag{10}$$

$$\mathcal{L}_{[{\rm Fe/H}]} = \frac{1}{\sqrt{2\pi}\,\sigma_{[{\rm Fe/H}]}} \cdot \exp\left\{-\frac{([{\rm Fe/H}]_{\rm obs} - [{\rm Fe/H}]_{\rm model})^2}{2\sigma_{[{\rm Fe/H}]}^2}\right\} \tag{11}$$

$$\mathcal{L}_{\nu} = \prod_{i=1}^{10} \left(\frac{1}{\sqrt{2\pi}\,\sigma_i(\nu)} \cdot \exp\left\{-\frac{(\nu_i^{\rm obs} - \nu_i^{\rm model})^2}{2\sigma_i^2(\nu)}\right\}\right). \tag{12}$$

In the above expression, $\nu_i^{\rm model}$ are the surface-term corrected frequencies of the models.

The values of likelihood function for model of KIC 8263801 as a function of mass, metallicity, age, and radius are shown in Figure 4. We choose the model that maximizes $\mathcal{L}$ as a candidate for the best-fit model. The model parameters are shown in Table 5. To clearly compare all of the theoretical frequencies of the best-fit model with observed frequencies, we show the échelle diagram of the best-fit model in Figure 5. In the figure, open symbols are the model frequencies corrected for the surface term, the filled symbols refer to the observable frequencies. Circles are used for $l = 0$ modes and squares for $l = 2$ modes.

Finally, we derive the parameters of star as the likelihood weighted mean and standard deviation from the models and obtain a mass of $M/M_{\odot} = 1.793 \pm 0.072$, age of $t = 1.48 \pm 0.21$ Gyr, and radius of $R/R_{\odot} = 10.53 \pm 0.28$. Our best-fit model has an age of 1.596 Gyr, the age as determined from the likelihood weighted average is not too different, and thus the question arises as to whether this star can be a member of NGC 6866. There are a number of results about the age of NGC 6866. For example, Loktin et al. (1994) derived $t = 0.66$ Gyr; Günes et al. (2012) obtained an age of $t = 0.8 \pm 0.1$ Gyr by 2MASS photometry; Kharchenko et al. (2005) obtained an age of $t = 0.5$ Gyr using an isochrone-based procedure; Bostanci et al. (2015) derived $t = 0.813 \pm 0.05$ Gyr with the metallicity of the cluster being about the solar value; Janes et al. (2014) derived age $t = 0.705 \pm 0.170$ Gyr; and Balona et al. (2013a) estimated the age as $t = 0.65 \pm 0.1$ Gyr with isochrones of solar composition. While the age estimates vary considerably, it is clear that the

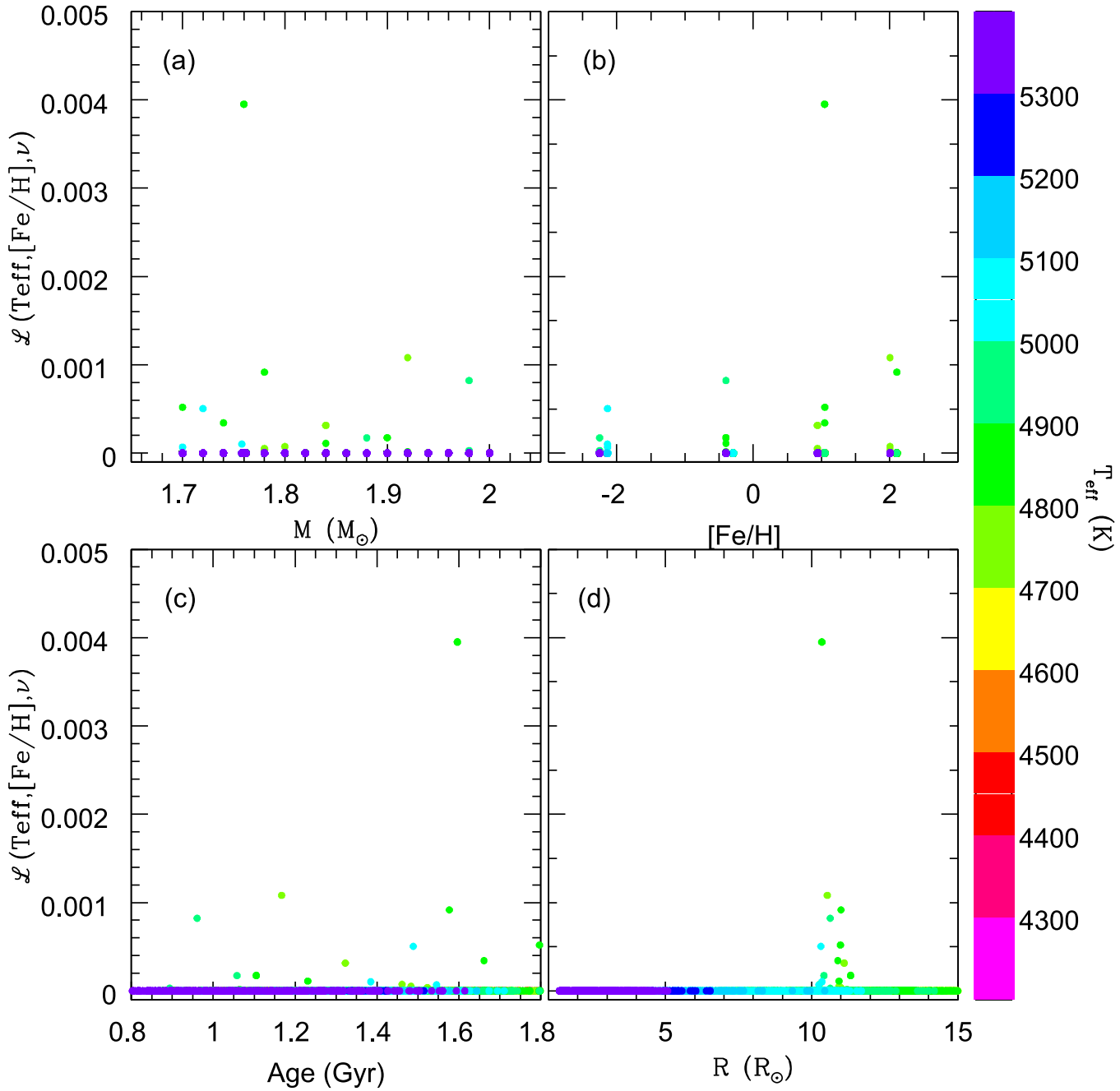

Figure 4. Likelihood values for models of KIC 8263801 as a function of mass, metallicity, age, and radius, corresponding to panels (a)–(d) respectively.

Table 5
The Parameters of the Best-fit Model

Model Parameters	Value
Mass ($M_{\odot}$)	1.76
Age (Gyr)	1.596
Effective temperature $T_{\rm eff}$ (K)	4884.3
Luminosity $\log L/L_{\odot}$	1.7384
$\log g$ (dex)	2.654
$\log R/R_{\odot}$	1.01487

consensus is that the age of NGC 6866 is less than 1 Gyr. Our age estimate of KIC 8263801 is significantly higher than 1 Gyr. Based on these results, we could conclude that KIC 8263801 is a nonmember of the cluster NGC 6866, which is consistent with Balona et al. (2013a).

We also derived the stellar parameters of KIC 8263801 using the Bayesian tool PARAM (da Silva et al. 2006; Rodrigues et al. 2014, 2017) and the grid models computed with MESA. The mode and its 68% credible intervals of the posterior probability density function as errors of parameters are mass $M/M_{\odot} = 1.8507^{+0.0721}_{-0.0249}$, age $t = 1.5844^{+0.1046}_{-0.1555}$ Gyr, radius $R/R_{\odot} = 10.5724^{+0.1414}_{-0.1185}$, and $\log g = 2.6544^{+0.003}_{-0.0048}$ dex. These results from PARAM are consistent with our above analysis ($M/M_{\odot} = 1.793 \pm 0.072$, age $t = 1.48 \pm 0.21$ Gyr, radius $\mathrm{R}/\mathrm{R}_{\odot} = 10.53 \pm 0.28$) within errors, and $\log g = 2.6544^{+0.003}_{-0.0048}$ dex is consistent with observation $\log\ g = 2.487 \pm 0.04$ dex within uncertainties.

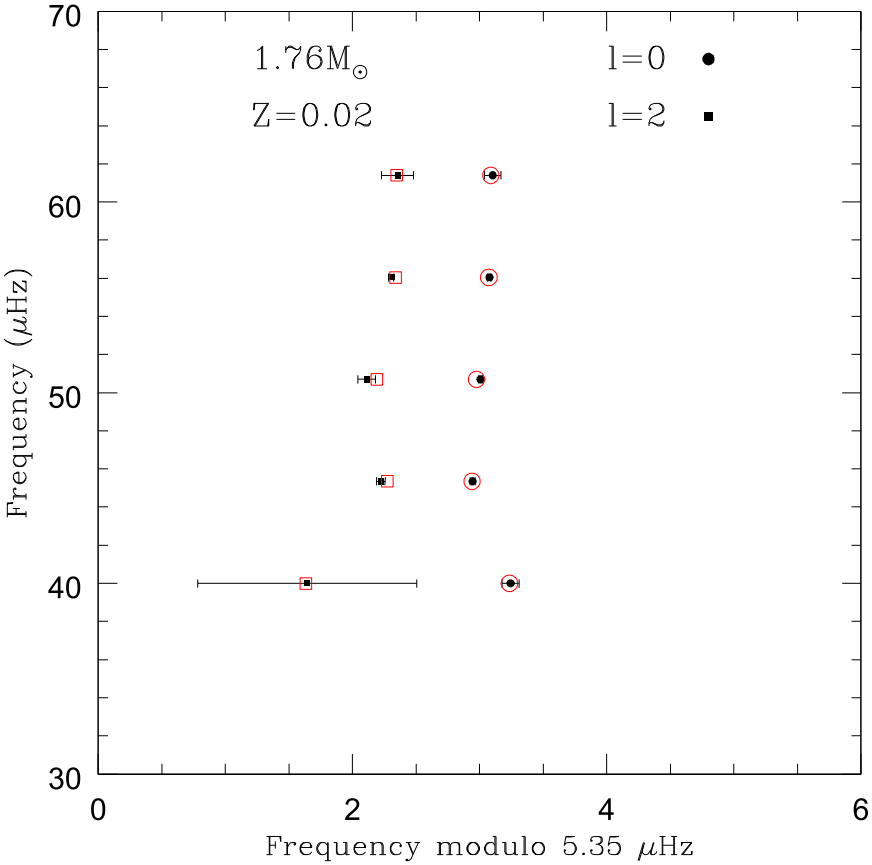

Figure 5. Échelle diagrams for the best-fit model. Open symbols are the surface-term corrected frequencies of the best-fit model; filled symbols refer to the observed frequencies. Circles are used for $l = 0$ modes, squares for $l = 2$ modes.

As mentioned above, and as is clear from Figure 3, red giants with inert helium cores and red giants with helium burning cores occupy a common region in the HR diagram. Errors in temperature and metallicity determinations make it difficult to unambiguously determine the evolutionary state, and hence age, of a red giant. Several asteroseismic tools have been developed to distinguish between the stars (Bedding et al. 2011; Kallinger et al. 2012; Elsworth et al. 2017). From the work presented above, we get the best-fit models of KIC 8263801 through modeling. The best-fit model of KIC 8263801 is a red-giant star, which implies that the star in question is on the ascending branch (hence it has an inert core). We use the technique of Kallinger et al. (2012) to confirm the result; the data do not have a high enough signal-to-noise ratio to use the observed $l = 1$ period spacing as suggested by Bedding et al. (2011), but they do have a signal-to-noise that is high enough to be able to determine mode frequencies making it unnecessary to use the method of Elsworth et al. (2017). The fact that we have good estimates of radial-mode frequencies makes the method of Kallinger et al. (2012) ideal.

Kallinger et al. (2012) found that the phase function ϵ determined around $\nu_{\max}$ could be used to distinguish between RGB and HeB stars. White et al. (2011) find that the phase shift ϵ changes with the evolutionary state of a star, and Kallinger et al. (2012) pointed out especially the central value of ϵ, which, given by the three radial modes around $\nu_{\max}$, contains the necessary information. In this work, we tested all of the above methods and found that considering the central radial modes like that of Kallinger et al. (2012) is suitable. Kallinger et al. (2012) expressed the three central radial order p modes by the following formula:

$$\nu_{c0} = \Delta\nu_c(n + \epsilon_c'), \tag{13}$$

where ν_{c0} is central frequency varying in the range $\nu_{\max} \pm 0.55\Delta\nu$ and $\Delta\nu_c$ is the separation between the three central modes. As explained by Rodrigues et al. (2017), to determine the large frequency properly, we use a weighted least squares fit to calculate an average large frequency separation $\langle\Delta\nu\rangle$. We use a Gaussian function, as described in Mosser et al. (2012) and Rodrigues et al. (2017), to calculate the individual weights:

$$\omega = \exp\left\{-\frac{(\nu - \nu_{\max})^2}{2\sigma^2}\right\} \tag{14}$$

where $\sigma = 0.66 \cdot \nu_{\max}^{0.88}$.

If ν_{c0} and $\Delta\nu_c$ are given, the phase shift of ϵ_c can be determined by the following formula defined by Kallinger et al. (2012):

$$\epsilon_c = \begin{cases} \epsilon_c' + 1 & \text{if } \epsilon_c' < 0.5 \text{ and } \Delta\nu > 3\mu\text{Hz} \\ \epsilon_c' & \text{otherwise} \end{cases} \tag{15}$$

with

$$\epsilon_c' = \left(\frac{\nu_{c0}}{\Delta\nu_c}\right) \mod 1. \tag{16}$$

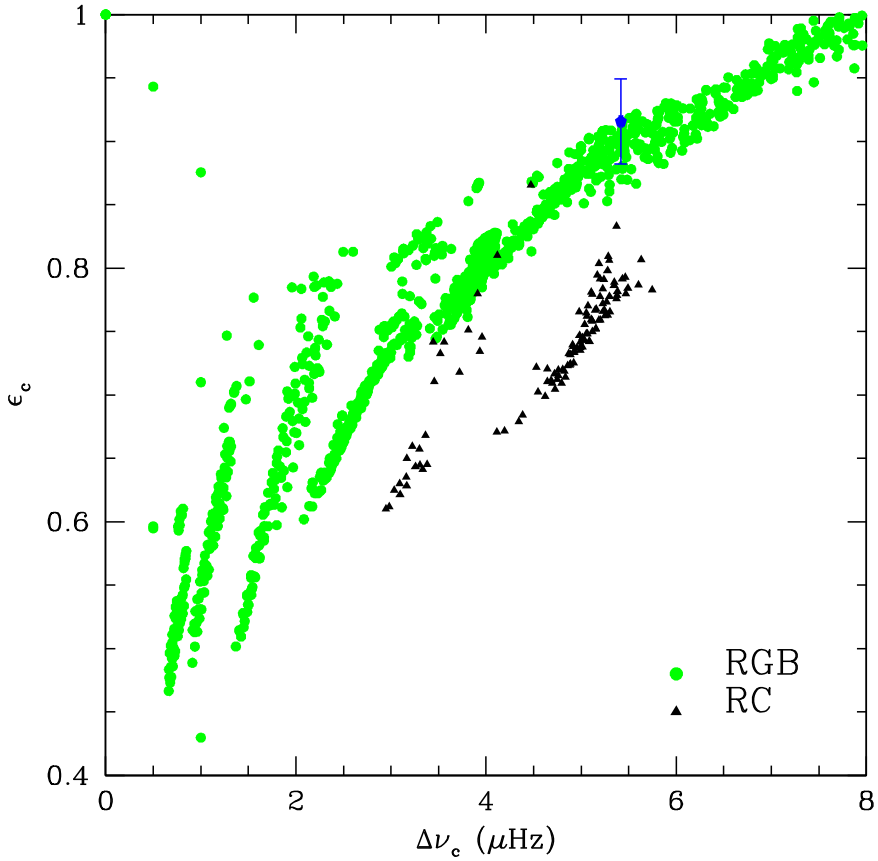

Figure 6. Central value of ϵ_c for models plotted against the large separation between the central modes. The (green) filled circles are RGB models, while the (black) filled triangles are RC models. The (blue) filled square with error-bars represents the observed result for KIC 8263801.

In Figure 6, we show the central value of ϵ_c for all the models from red giants to red clump stars (with $\Delta\nu_c \leqslant 8\ \mu$Hz) along the evolutionary track, which are calculated using the input parameters in Table 4. Figure 6 displays the ϵ_c against the large separation between the central modes. The stars clearly divide into different groups, where the circles are RGB models while the triangles are HeB models. The (blue) square in the figure denotes the observed value of ϵ_c with the error bar of the star, obtained by error propagation analysis. We thus find that the KIC 8263801 is indeed an inert-core RGB star. Although Abedigamba (2016) had used the median gravity-mode period spacing ΔP of $l = 1$ modes to determine that KIC 8263801 is a helium-burning SRC star, we believe that the low SNR of the data affected the value of ΔP obtained by them. Given the mass of the best-fit model, ΔP would be the most reliable way of determining the evolutionary state of this star if measured properly (see Bedding et al. 2011). However, KIC 8263801 has a $\Delta\nu_c$ of about 5.35 μHz, and in that region of Figure 6, the two stages of evolution are well separated.

5. Conclusions

We have performed an asteroseismic study of the star KIC 8263801 in order to determine its age, evolutionary status, and membership or otherwise in the open cluster NGC 6866. Our best-fit models have mass $M/M_\odot = 1.76$, age $t = 1.596$ Gyr, and radius $R/R_\odot = 10.3483$, while a full grid analysis gives $M/M_\odot = 1.793 \pm 0.072$, age $t = 1.48 \pm 0.21$ Gyr, and radius $R/R_\odot = 10.53 \pm 0.28$.

The best-fit model of KIC 8263801 is on the ascending part of the red-giant branch, making it likely that KIC 8263801 is also in that state. We confirm this using the $\epsilon_c - \Delta\nu_c$ diagram.

The age estimates of KIC 8263801 make it unlikely to be a member cluster NGC 6866, despite being in the same field since NGC 6866 has age estimates below 1 Gyr. This result is consistent with that of Balona et al. (2013a).

Y.K.T. and N.G. acknowledge the research grant from the National Natural Science Foundation of China (grant No. 11673005). S.B. acknowledges NSF grant AST-1514676 and NASA grant NNX16AI09G. E.P.B. acknowledges support from the European Research Council under the European Community's Seventh Framework Programme (FP7/2007-2013)/ERC grant agreement No. 338251 (StellarAges) and the National Physical Science Consortium (NPSC) Fellowship.

ORCID iDs

Yanke Tang https://orcid.org/0000-0003-4207-1694
Sarbani Basu https://orcid.org/0000-0002-6163-3472
Guy R. Davies https://orcid.org/0000-0002-4290-7351
Earl P. Bellinger https://orcid.org/0000-0003-4456-4863
Ning Gai https://orcid.org/0000-0002-9308-587X

References

Abedigamba, O. P. 2016, NewA, 46, 21
Ball, W. H., & Gizon, L. 2014, A&A, 568, A123
Balona, L. A., Joshi, S., Joshi, Y. C., & Sagar, R. 2013a, MNRAS, 429, 1466

Balona, L. A., Medupe, T., Abedigamba, O. P., et al. 2013b, MNRAS, 430, 3472
Basu, S., Chaplin, W. J., & Elsworth, Y. 2010a, ApJ, 710, 1596
Basu, S., Chaplin, W. J., & Elsworth, Y. 2010b, Ap&SS, 328, 79
Basu, S., Grundahl, F., Stello, D., et al. 2011, ApJ, 729, 10
Beck, P. G., Bedding, T. R., Mosser, B., et al. 2011, Sci, 332, 205
Bedding, T. R. 2014, in Asteroseismology: XXII Canary Islands Winter School of Astrophysics, ed. P. L. Pallé & C. Esteban (Cambridge: Cambridge Univ. Press), 60
Bedding, T. R., Huber, D., Stello, D., et al. 2010, ApJL, 713, L176
Bedding, T. R., Mosser, B., Huber, D., et al. 2011, Natur, 471, 608
Bellinger, E. P., Angelou, G. C., Hekker, S., et al. 2016, ApJ, 830, 31
Bellinger, E. P., Angelou, G. C., Hekker, S., et al. 2017, EPJWC, 160, 05003
Borucki, W., Koch, D., & Batalha, N. 2009, in Proc. IAU Symp. 253, Transiting Planets, ed. F. Pont, D. Sasselov, & M. Holman (Cambridge: Cambridge Univ. Press), 289
Borucki, W. J., Koch, D., Basri, G., et al. 2010, Sci, 327, 977
Bostanci, Z. F., Ak, T., Yontan, T., et al. 2015, MNRAS, 453, 1095
Brown, T. M., Gilliland, R. L., Noyes, R. W., & Ramsey, L. W. 1991, ApJ, 368, 599
Brown, T. M., Latham, D. W., Everett, M. E., & Esquerdo, G. A. 2011, AJ, 142, 112
Chaplin, W. J., Basu, S., Huber, D., et al. 2014a, ApJS, 210, 1
Chaplin, W. J., Elsworth, Y., Davies, G. R., et al. 2014b, MNRAS, 445, 946
Chaplin, W. J., Kjeldsen, H., Christensen-Dalsgaard, J., et al. 2011, Sci, 332, 213
Christensen-Dalsgaard, J. 1984, in Space Research in Stellar Activity and Variability, ed. A. Mangeney & F. Praderie (Meudon: Paris Observatory Press), 11
Cox, J. P., & Giuli, R. T. 1968, Principles of Stellar Structure (New York: Gordon and Breach)
da Silva, L., Girardi, L., Pasquini, L., et al. 2006, A&A, 458, 609
Davies, G. R., Aguirre, V. S., Bedding, T. R., et al. 2016, MNRAS, 456, 2183
Davies, G. R., & Miglio, A. 2016, AN, 337, 774
Demarque, P., Woo, J.-H., Kim, Y.-C., & Yi, S. K. 2004, ApJS, 155, 667
De Ridder, J., Barban, C., Baudin, F., et al. 2009, Natur, 459, 398
Elsworth, Y., Hekker, S., Basu, S., & Davies, G. 2017, MNRAS, 466, 3344
Gai, N., Basu, S., Chaplin, W. J., & Elsworth, Y. 2011, ApJ, 730, 63
Gilliland, R. L., Brown, T. M., Christensen-Dalsgaard, J., et al. 2010, PASP, 122, 131
Grevesse, N., & Sauval, A. J. 1998, SSRv, 85, 161
Gualme, P., McKeever, J., Jackiewicz, J., et al. 2016, ApJ, 832, 121
Guggenberger, E., Hekker, S., Angelou, G., et al. 2016, MNRAS, 470, 2069
Guggenberger, E., Hekker, S., Basu, S., et al. 2016, MNRAS, 460, 4277
Günes, O., Karatas, Y., & Bonatto, C. 2012, NewA, 17, 720
Handberg, R., & Lund, M. N. 2014, MNRAS, 445, 2698
Handberg, R., & Lund, M. N. 2017, A&A, 597, A36
Hoag, A. A., Johnson, H. L., Iriarte, B., et al. 1961, PUSNO, 17, 343
Huber, D., Bedding, T. R., Stello, D., et al. 2011, ApJ, 743, 143
Huber, D., Silva Aguirre, V., Matthews, J. M., et al. 2014, ApJS, 211, 2
Huber, D., Stello, D., Bedding, T. R., et al. 2009, CoAst, 160, 74
Janes, K., Barnes, S. A., Meibom, S., & Hoq, S. 2014, AJ, 147, 139
Kallinger, T., Hekker, S., Mosser, B., et al. 2012, A&A, 541, A51
Kharchenko, N. V., Piskunov, A. E., & Röser, S. 2005, A&A, 438, 1163
Kjeldsen, H., & Bedding, T. R. 1995, A&A, 293, 87
Kjeldsen, H., Bedding, T. R., & Christensen-Dalsgaard, J. 2008, ApJL, 683, L175
Koch, D. G., Borucki, W. J., Basri, G., et al. 2010, ApJL, 713, L79
Loktin, A. V., Matkin, N. V., & Gerasimenko, T. P. 1994, A&AT, 4, 153
Mosser, B., Elsworth, Y., Hekker, S., et al. 2012, A&A, 537, A30
Paxton, B., Bildsten, L., Dotter, A., et al. 2011, ApJS, 192, 3
Paxton, B., Cantiello, M., Arras, P., et al. 2013, ApJS, 208, 4
Pinsonneault, M. H., Elsworth, Y., Epstein, C., et al. 2014, ApJS, 215, 19
Rodrigues, T. S., Bossini, D., Miglio, A., et al. 2017, MNRAS, 467, 1433
Rodrigues, T. S., Girardi, L., Miglio, A., et al. 2014, MNRAS, 445, 2758
Schmitt, J. R., & Basu, S. 2015, ApJ, 808, 123
Silva Aguirre, V., Davies, G. R., Basu, S., et al. 2015, MNRAS, 452, 2127
Silva Aguirre, V., Lund, M. N., Antia, H. M., et al. 2017, ApJ, 835, 173
Stello, D., Meibom, S., Gilliland, R. L., et al. 2011, ApJ, 739, 13
Tang, Y. K., Bi, S. L., & Gai, N. 2008b, NewA, 13, 541
Tang, Y. K., Bi, S. L., Gai, N., & Xu, H. Y. 2008a, ChJA&A, 8, 421
Tang, Y. K., & Gai, N. 2011, A&A, 526, A35
Tassoul, M. 1980, ApJS, 43, 469
Townsend, R. H. D., & Teitler, S. A. 2013, MNRAS, 435, 3406
White, T. R., Bedding, T. R., Stello, D., et al. 2011, ApJ, 743, 161
Wu, T., & Li, Y. 2016, ApJL, 818, L13
Yildiz, M., Çelik Orhan, Z., örtel, S., & Roth, M. 2017, MNRAS, 470, L25